ADVANCED ELECTRONIC MATERIALS Open Access
www.advelectronicmat.de

Plant-Based Electrodes for Bioimpedance Readings of Fruit

Saleh Hamed, Pietro Ibba, Antonio Altana, Camilla Rinaldi, Paolo Lugli, Luisa Petti, Athanassia Athanassiou,* Danila Merino,* and Pietro Cataldi**

Waste management, particularly electronic waste, presents significant environmental challenges. Similarly, agricultural and food waste, produced in large quantities, also imposes considerable disposal and processing costs. Addressing both of these issues, this study explores the potential of creating environmentally friendly electronic materials from renewable resources derived from agricultural byproducts. Specifically, sustainable electronic conductors are developed by converting tomato plant waste into conductive, biodegradable materials. This is achieved by integrating graphene nanoplatelets (GnPs) with hydrolyzed tomato waste in bio-based latex matrices using water-based methods. Importantly, the use of hydrolyzed tomato waste without the need for isolating specific components represents a whole-biomass utilization strategy. This approach simplifies processing while maximizing the valorization of agricultural waste. The resulting latex–tomato waste composite containing 20 wt.% GnPs exhibits satisfying mechanical properties and moisture resistance, along with a resistivity of 0.46 Ω · m. Notably, it serves effectively as an electrode for recording the bioimpedance of fruits. These findings demonstrate the potential of this material as a sustainable alternative for green electronics, while simultaneously contributing to the reduction of both electronic and agricultural waste within a circular economy framework.

1. Introduction

Electronics lays the foundation for established and ubiquitous devices like smartphones and computers. Contemporarily, it supports the evolution of disrupting fields like artificial intelligence, enabling it to process larger datasets and perform more complex tasks. Nevertheless, the success of electronics comes with significant drawbacks. Indeed, electronics production and disposal pose significant environmental challenges, ranging from material supply and toxicity to escalating issues of electronic waste (*e*-waste) management.[1–3] The 2024 report on global *e*-waste production[4] highlights that a record 62 million tons of this kind of waste was generated in 2022. Alarmingly, only around 20% of this waste was recycled since electronics were developed on a linear economy model, where products are made, used, and discarded without considering sustainability or circularity.[5,6] This unsustainable approach is projected to exacerbate the accumulation of *e*-waste, reaching 120 million metric tons per year in 2050.[7] As such, there is a growing interest in sustainable materials for creating "green" electronics, meaning devices made with biobased, biodegradable, and/or recyclable materials to reduce the environmental impact of electronics.[1–3] At the same time, agricultural residues also present societal and environmental challenges. Such waste class is estimated to produce a staggering 10 billion tons annually,[8] posing a significant disposal problem. Thus, they are often treated improperly and incinerated, producing greenhouse gases and toxic substances that poison the environment.[9,10] Plant-derived waste represents a more significant share (around 60%) of the whole food supply chain than animal-derived ones.[11] These residues contain useful substances such as carbohydrates, proteins, lipids, and minerals.[11] Thus, novel processes can transform these compounds into valuable products.[11] For example, plant-based waste has been converted into biofuels[12] and bioplastics,[13] used for composting[14] and construction materials,[15] and processed into animal feed.[16] Recently, they were also used in high-value applications such as the production of pharmaceuticals.[17,18]

This abundance of agricultural waste presents a unique opportunity. Indeed, by re-purposing such class of waste as raw materials for electronics to make insulators/dielectrics, conductors, and semiconductors, we can address two critical issues

S. Hamed, C. Rinaldi, A. Athanassiou, D. Merino[+], P. Cataldi
Smart Materials
Istituto Italiano di Tecnologia
Via Morego 30, Genova 16163, Italy
E-mail: athanassia.athanassiou@iit.it; danila.merino@ehu.eus; pietro.cataldi@iit.it

S. Hamed, P. Ibba, A. Altana, P. Lugli, L. Petti
Faculty of Engineering
Free University of Bozen-Bolzano
Via Bruno Buozzi 1, Bozen-Bolzano 39100, Italy
E-mail: luisa.petti@unibz.it

L. Petti
Competence Center for Plant Health
Free University of Bozen-Bolzano
Piazza Università 5, 39100 Bolzano, Italy

The ORCID identification number(s) for the author(s) of this article can be found under https://doi.org/10.1002/aelm.202500109

[+]Present address: Sustainable Biocomposite Materials (SusBioComp), Basque Center for Macromolecular Design and Engineering (POLYMAT), University of the Basque Country UPV/EHU, Avenida de Tolosa 72, Donostia-San Sebastian 20018, Spain

DOI: 10.1002/aelm.202500109

simultaneously: increasing electronic sustainability and reducing the environmental impact of agricultural residues.[19,20] In this way, we can pose the basis of the circular economy approach in the electronics sector, manufacturing agricultural waste-based materials for high-value applications.

Agricultural waste-based insulators and dielectrics are numerous. Among the most common are cellulosic ones, such as bagasse from sugarcane and other biomasses, which are processed as fibrillated cellulose micro or nanosized.[21,22] Such materials are used in printed electronics as a flexible substrate acting as an insulator/dielectric material,[23] a transparent substrate in the form of nanosized fibers,[23–25] and a substrate modifier to smooth roughness.[23] Other waste-derived substrates for electronics are collagen[26] and chitin[20] for implantable and flexible electronics,[27] respectively.

On the other hand, conductors and semiconductors derived from waste are rarer. Waste-based conductors have been developed based on ionically[28–31] or electronically conductive materials.[19,32] Ionic ones are typically based on hydrogels made of gelatin extracted from animal skins,[33,34] alginate obtained from seaweed,[35] and chitin derived from crustacean shells,[36,37] and exhibit appealing properties such as self-healing, biocompatibility, degradability, softness, and, sometimes, recyclability.[38,39] However, waste-based conductive hydrogels conduct ions and cannot sustain a constant electronic current in a circuit.[40] Their correct functioning relies on hydration and thus strongly depends on the surrounding environment. Ionically conductive materials such as gelatin have been doped with electrically conductive fillers and polymers[41] such as reduced graphene oxide,[41] carbon nanotubes,[34] and silver nanoflakes[42] to counterbalance such issues, obtaining transient conductors, suitable for application needing a limited time stability outdoors. On the other hand, electrically conductive waste-based materials are typically obtained following a carbonization processes. For example, residues from plants, such as peanuts,[43] melon,[44] asparagus,[45] flour,[46] oil palm,[47] seaweed,[48] and rice,[49,50] or animals, such as shrimp and crab shells,[50–52] were carbonized. The resulting materials are carbon-based powders such as graphene-related materials,[51,53,54] activated carbon,[45] carbon black,[47] or carbon nanofibers.[55] Such materials are mostly blended with long-lasting, petroleum-derived binders and used as electrodes in energy storage applications,[53,56–58] typically for making supercapacitors.[46,48,49,51,52,59] Nevertheless, carbonization is a high energy-demanding process since required temperatures are normally 300–600°C to achieve high-quality carbon materials. Another approach consists of valorizing fibrous cellulose remnants by functionalization with conductive polymers to obtain conductors for flexible[60] and wearable[61] electronics. A less investigated strategy to make waste-based conductors involves the extraction of binders from agricultural residues, such as keratin[19] from wool clips or zein[32] derived from byproducts of corn processing, and use them in conductive ink formulations, including nanocarbon conductive fillers.

However, these last two examples involve extraction procedures from biomass, which add complexity to waste valorization. Furthermore, such extraction methods can generate additional waste throughout the process. A suitable and more sustainable approach would be to develop conductive materials using the biomass entirely, maximizing the residues employment. In this work, we focus on using tomato plant waste (TW), which represents a valuable resource.[62] Global tomato cultivation produces significant waste, with approximately 15 tons per hectare of fresh plant residues generated annually.[63] These residues, rich in cellulose, hemicellulose, and lignin, offer potential for value addition and bioplastic film production. Yet, due to their chemical composition, TW is hydrophilic and non-conductive, requiring chemical modification to enhance its properties.

To address these challenges, TW can undergo a hydrolysis process, which deconstructs the vegetable cell wall and releases its constituent polymers into the medium, using water and mild acidic or alkaline conditions.[64–66] However, even after this treatment, further enhancement of TW's mechanical properties and moisture resistance is required. To achieve this, TW are combined with natural rubber, also known as latex, to form a composite material with enhanced properties. Latex, derived from *Hevea brasiliensis*, is known for its elasticity and resilience, making it an ideal candidate for this purpose with the possibility of obtaining biobased flexible materials. In addition, graphene nanoplatelets (GnPs) are incorporated using a simple one-step water-based, environmentally friendly fabrication method to introduce electrical conductivity. Such nanofiller is selected since it is a broadly available graphitic material made up of nanoflakes with nanometric thickness and micrometric lateral dimension that have attributes halfway between graphite and single-layer graphene.[67] In contrast to tube-like or spherical carbon nanofillers, GnPs offer a well-balanced mix of electrical conductivity, suitable barrier, and mechanical properties, ease of processing, and cost-effectiveness (i.e., less than 0.1 $/g[6,68]), which is why we chose them as carbon-based fillers. Because of these characteristics, GnPs are ideal for various electronic applications that need satisfying electrical conduction properties while maintaining a moderate price and a potential large-scale production.

Nowadays, fruit monitoring technologies rely on smart labels with time-temperature indicators or gas sensors on the packaging.[69,70] Bioimpedance has proved to potentially provide more precise and quantitative tracking of fruit aging across the supply chain.[40] The contact electrodes, usually Ag/AgCl types designed for biomedical applications, are essential to this technique. However, due to the high cost and impracticality of Ag/AgCl electrodes, they are unsuitable for widespread, cost-effective food monitoring applications.[40]

This research aims to harness the combined advantages of TW, latex, and GnPs to develop conductive, environmentally sustainable composites produced through water-based procedure for use in green electronics. Specifically, these materials are employed as electrodes for bioimpedance measurements to monitor fruit ripening, enabling in the long term precise harvesting and quality control of fruit without damaging the product.[71–76] This research promotes a circular economy and sustainability by converting agricultural residues into electrodes for bioimpedance-based fruit ripening monitoring, offering a non-destructive, real-time method to assess fruit maturity. Using TW, latex, and GnPs to create an eco-friendly conductive material, we reduce both *e*-waste and agricultural waste while advancing sustainable green electronics and lessening dependency on non-renewable resources.

The latex–tomato waste composite with 20 wt.% GnPs demonstrates good mechanical properties and moisture absorbtion with

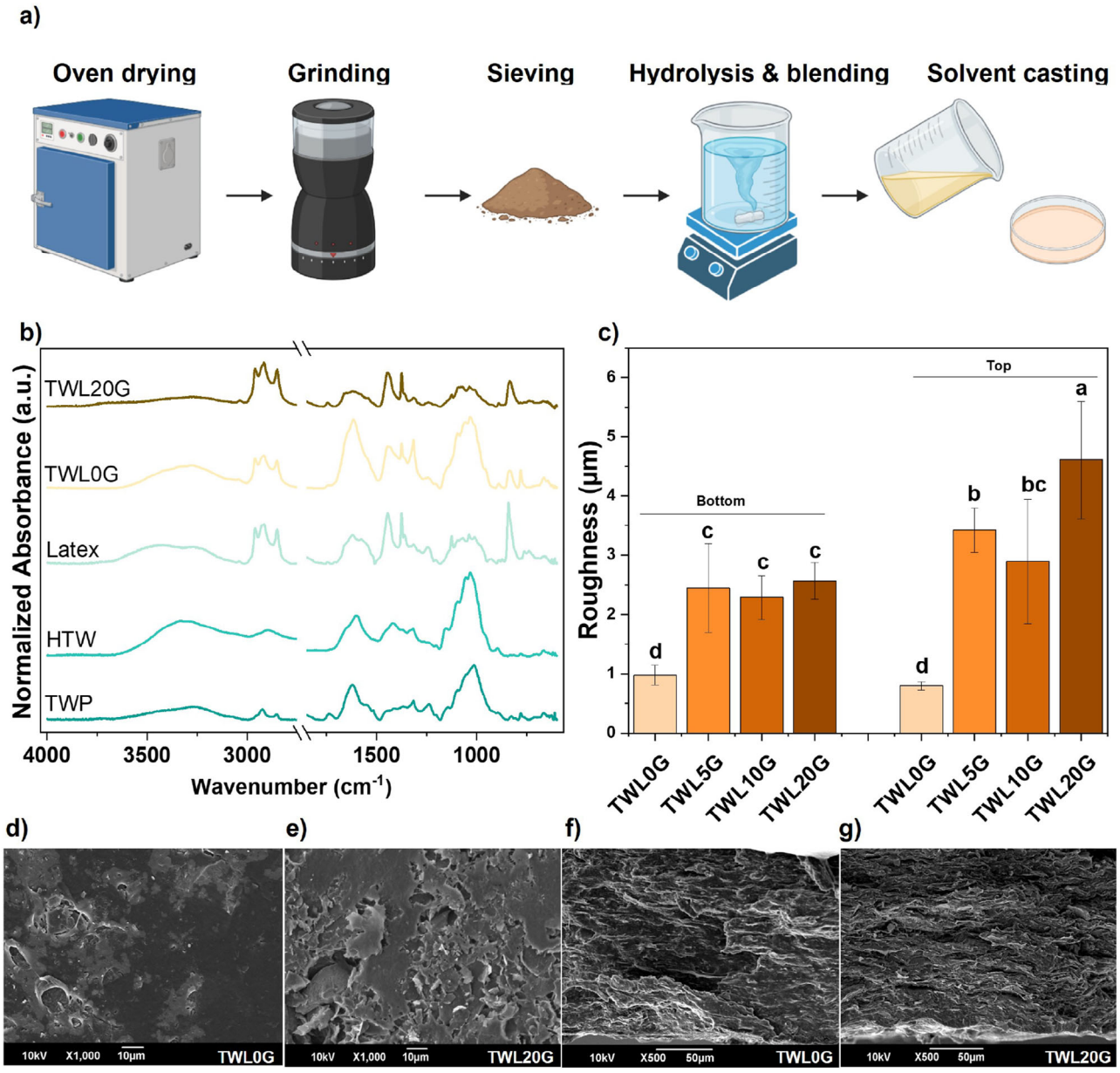

Figure 1. Overview of Material Preparation and Physicochemical and Morphological Characterization of the Tomato Waste Latex (TWL) Composites. a) Preparation steps for TWL composites; b) FTIR analysis of the materials; c) Roughness measurements comparing the bottom and top surfaces of the composites; d) SEM images of the TWL0G (0% GnPs) surface; e) SEM images of the TWL20G (20% GnPs) surface; f) SEM images of the TWL0G cross-section; g) SEM images of the TWL20G cross-section. Lowercase letters inside panel c) indicate whether the results are significantly different (different letters denote statistically different results) with a 95% confidence.

a resistivity of 0.46 Ω · m. It functions as a bioimpedance electrode for over 160 continuous hours. The composite quickly degrades in seawater. These properties highlight its potential for plant monitoring.

2. Results and Discussion

TW was processed as illustrated in **Figure** 1a. Following oven-drying, grinding, and sieving to obtain a fine powder, the material underwent hydrolysis and was subsequently mixed with latex in equal parts by weight. This mixture was cast into films using the solvent casting method. To enhance conductivity, GnPs were incorporated into the TW-latex (TWL) mixture at concentrations of 5, 10, and 20 wt.% as shown in **Table** 1. The films were analyzed using Attenuated Total Reflectance-Fourier Transform Infrared (ATR-FTIR) Spectroscopy. The FTIR spectra for latex, tomato waste powder (TWP), hydrolyzed tomato waste (HTW), and the composite films—TWL0G (without GnPs) and TWL20G (with 20 wt.% GnPs)—are presented in Figure 1b.

Table 1. Component percentages in samples—including graphene nanoplatelets (GNPs), tomato waste (TW), and latex.

Sample	GNPs [%]	TW [%]	Latex [%]
TWL0G	0	50	50
TWL5G	5	47.5	47.5
TWL10G	10	45	45
TWL20G	20	40	40
Latex	0	0	100

The major constituent of natural rubber (latex) is *cis*-1,4-polyisoprene, which accounts for approximately 94% of the material's weight. The remaining 6% consists of non-rubber compounds, including lipids (1.5–3% w/w), proteins and polypeptides (2% w/w), carbohydrates (0.4% w/w), and minerals (0.2% w/w).[77] Key peaks for latex were identified in the region of 3030–2800 cm^{-1}, corresponding to ν C═C–H, asymmetric stretching of CH_3 and CH_2 groups, and symmetric stretching of CH_3 and CH_2 groups. The absorption band at 1647 cm^{-1} is attributed to ν C═C in *cis*-1,4-polyisoprene, while the out-of-plane bending mode for = CH was observed at 873 cm^{-1} (γ C═C–H, indicating the presence of the *cis* isomer). Peaks at 1630 cm^{-1} and 1541 cm^{-1} correspond to Amide I (ν R_1–(C═O)–NH–R_2) and Amide II (β N–H + ν C–N), respectively, indicating protein presence, along with a small broad peak between 3500 and 3000 cm^{-1} attributed to ν N–H from proteins.[78] For TWP and HTW, characteristic peaks included ν OH at 3270 cm^{-1}, ν CH at 2928 cm^{-1}, and ν C–O–C at 1035 cm^{-1}, indicative of carbohydrate presence.[79] These peaks were consistent across all TW samples. The main difference between TWP and HTW is the increased intensity of the OH peak in HTW, reflecting the increased OH content expected after hydrolysis, aligning with findings from the literature on hydrolyzed biomass.[64–66]

The FTIR spectra of TWL0G exhibited a combination of peaks from both latex and tomato waste, with a shift of the OH peak to lower wavenumbers suggesting hydrogen bonding interactions between the components. Notably, the addition of 20 wt.% GnPs did not significantly alter the observed FTIR spectrum, as GnPs, which lack oxygen-containing groups, displayed a flat FTIR spectrum consistent with prior reports.[80]

The roughness analysis presented in Figure 1c highlights distinct differences between the top and bottom surfaces of the composite films. For TWL0G, which lacks GnPs, both surfaces exhibited a roughness in the order of 1 µm, the lowest and most uniform roughness compared to the GnP-containing samples. In contrast, the GnP-containing composites (TWL5G, TWL10G, and TWL20G) displayed two different bottom and top roughness profiles. The bottom surfaces of these films were notably smoother, with a roughness around 2.5 µm, likely due to the influence of the casting plate during film formation. However, the top surfaces exhibited increasing roughness with higher GnPs content, particularly in TWL20G, which reached 4.5 µm. This trend suggests that as the GnPs concentration increases, particle aggregation or uneven distribution may contribute to the formation of a rougher top surface.

To gain deeper insights into the film morphology, we conducted Scanning Electron Microscopy (SEM) analysis on both the surface topographies and cross-section of the films. SEM images are presented in Figure 1 (d-g). The top morphologies in Figure 1d, 1e and S3a indicated a more homogeneous and smooth surface of the TWL0G compared to the TWL20G sample, respectively, confirming the roughness measurements of Figure 1c. On the other hand, analyzing the cross-section images presented in Figure 1f,g and Figure S3b, significant differences were observed. The cross-section of TWL0G (Figure 1f) revealed a rough and uneven structure with visible voids or pores, suggesting a loosely packed polymer matrix with irregular morphology. In contrast, the cross-section of TWL20G (Figure 1g; Figure S3b in Supporting Information) demonstrated a smoother and more compact structure. The incorporation of GnPs into the TWL20G sample likely enhanced the matrix's structural uniformity and reduced porosity, as evidenced by the denser and more cohesive morphology. While GnPs increase roughness on the film's outer surface by forming micro asperities, they simultaneously densify the bulk, yielding a more compact and uniform cross section compared with the GnP free sample.

Understanding mechanical properties is essential for evaluating the performance of composite materials. These properties influence how a material responds to stress, its durability, and its potential applications. In the case of TWL composites, factors such as stiffness, strength, and flexibility help determine their suitability for practical use. The properties of the TWL compounds, specifically elastic modulus, tensile strength, and elongation at break, were evaluated as a function of the GnP content, as illustrated in **Figure 2**a–c.

Incorporating TW into pure latex markedly alters its mechanical properties. Elastic modulus of pure latex, initially at 0.33 ± 0.10 MPa (Figure S1, Supporting Information), experiences a substantial increase upon the addition of TW, reaching an average of 175.12 ± 5.70 MPa in the TWL0G composite (Figure 2a). This significant enhancement indicates that TW serves as an effective reinforcing filler, augmenting the stiffness of the material.

The mechanical properties are further tuned with the inclusion of GnPs. As illustrated in Figure 2a and Figure S2 (Supporting Information), the elastic modulus of the TWL composites rises to 767.58 ± 92.70 MPa for TWL20G. This nearly fourfold increase underscores the efficacy of GnPs in reinforcing the composite films.

Similarly, the maximum tensile strength shows notable improvement. Pure latex exhibits a tensile strength of 1.66 ± 0.28 MPa, as shown in Figure S1 (Supporting Information). As shown in Figure S2 (Supporting Information), the addition of TW elevates the tensile strength to 4.53 ± 0.30 MPa in the TWL0G sample, demonstrating TW's contribution to the material's strength. With the incorporation of GnPs, the tensile strength doubles, reaching 10.42 ± 0.47 MPa for TWL20G, as shown in Figure 2b. This progression highlights the augmented strength achieved with higher GnP concentrations.

In contrast, the elongation at break decreases with the addition of both TW and GnPs. Pure latex displays an elongation at break of 1355.5% ± 137.90% (Figure S1 Supporting Information), indicating high stretchability. Incorporating TW reduces this value significantly to approximately 30.60% ± 0.56% in the TWL0G sample, as shown in Figure S2 (Supporting Information). The presence of GnPs further diminishes the elongation at break, dropping to 1.50% ± 0.25% for TWL20G, as depicted in Figure 2c.

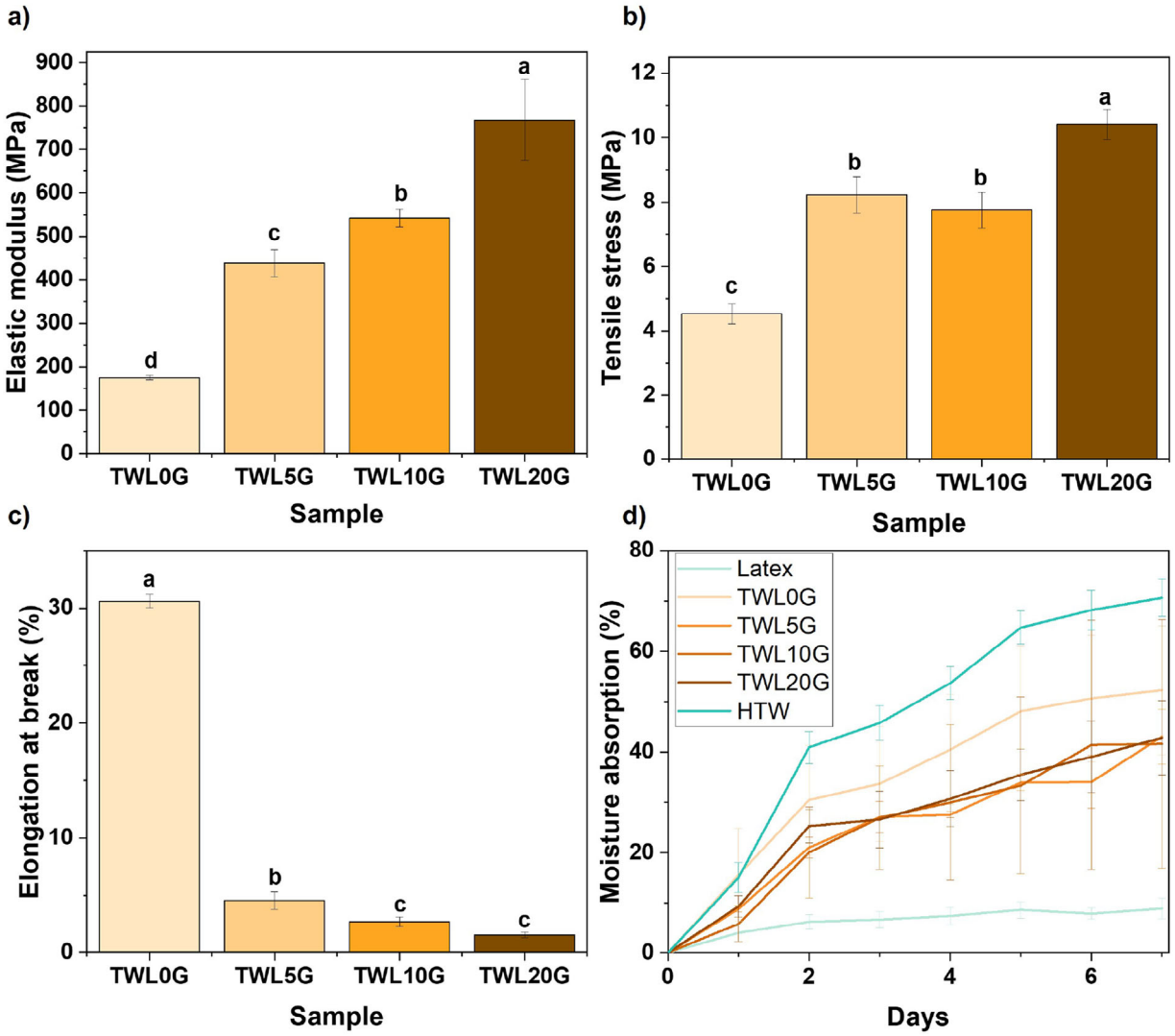

Figure 2. Mechanical Properties and Water Interaction of the Tomato Waste-Latex (TWL) Composites. a) Elastic Modulus (MPa) of TWL composites as a function of GnPs content; b) Tensile Strength (MPa) with varying GnPs concentrations; c) Elongation at Break (%) as a function of GnPs content; d) Moisture absorption (%) as a function of time for the films of Latex, HTW and their composites with GnPs. Lowercase letters inside panels (a–c) indicate whether the results are significantly different (different letters denote statistically different results) with a 95% confidence.

This reduction is attributed to the GnPs, which limit the latex chain ability to deform under stress.

These observations align with established literature on rubbery materials reinforced with carbon-based fillers, where increased elastic modulus and tensile strength coupled with decreased elongation at break are common phenomena.[81,82] The decrease in elongation at break is often due to the strain amplification effect and stress concentration at filler agglomerates, creating weak spots where stress accumulates, leading to cracking or damage under load.[83]

In light of the potential application of these materials in real-world green-electronics, it is crucial to understand their interactions with humid environments, as this knowledge is essential to ensure their long-term stability, performance, and reliability under varying environmental conditions. To address this, we examined the moisture absorption behavior of the prepared bio-composites in a 100% relative humidity (RH) environment, representing extreme humid conditions and serving as a worst-case scenario. Figure 2d illustrates the moisture absorption profiles of various composite materials: latex, HTW, TWL0G, TWL5G, TWL10G, and TWL20G.

As shown, HTW exhibits the highest moisture absorption, with a steep increase in moisture uptake during the initial days, eventually stabilizing between 60% and 70%. This behavior is consistent with the high content of hydrophilic compounds in the biomass,[20,84] which facilitates water absorption. On the other hand, Latex displays the lowest moisture absorption, with a nearly flat profile throughout the experiment. After one week, it absorbs only about 9% of its initial dry weight, indicating its strong resistance to moisture due to its hydrophobic nature. The composite TWL0G, which combines Latex and HTW in equal proportions, shows intermediate behavior. Its moisture absorption

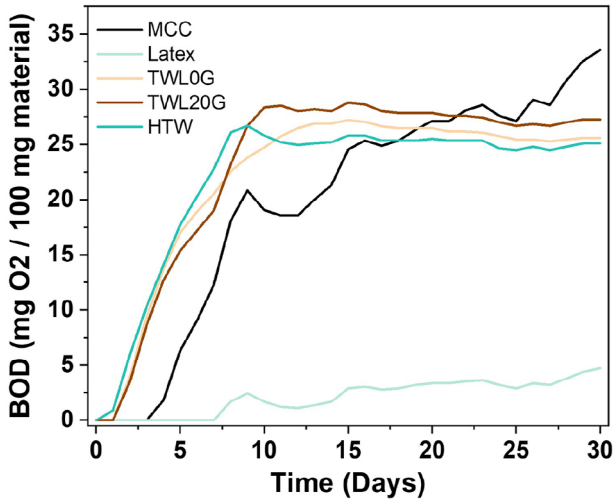

Figure 3. Biochemical Oxygen Demand (BOD) tests, measured in mg O_2 per 100 g of material, over time (days) for Tomato Waste-Latex (TWL) compositions, latex, hydrolyzed tomato waste (HTW) and microcrystalline cellulose (MCC) controls.

is higher than the Latex sample but lower than the HTW sample, reaching about 50% after one week. The presence of both hydrophilic and hydrophobic components results in this moderate moisture uptake. The other TWL formulations containing GnPs (TWL5G, TWL10G, and TWL20G) show progressively reduced moisture absorption compared to HTW, with all samples stabilizing at around 40% moisture absorption after one week. Interestingly, there is no significant difference in moisture absorption between the samples with 5%, 10%, and 20% GnPs, indicating that the addition of GnPs helps to stabilize moisture absorption but further increases in GnPs content do not lead to substantial differences in behavior.

These trends emphasize the role of GnPs in reducing the hygroscopicity of the biocomposites. Due to their predominantly hydrophobic nature, GnPs exhibit strong van der Waals forces and pi-pi interactions, which limit water interaction. Additionally, their high aspect ratio and flake-like structure enhance gas barrier properties compared to composites without GnPs.[85,86]

The biodegradability of the electrodes was assessed in seawater following ISO 23977-2:2020, which standardizes the determination of biochemical oxygen demand (BOD) for plastic materials.[2,6] Seawater is a relevant test environment, as common biopolymers such as polylactic acid, polyhydroxybutyrate, and polycaprolactone degrade more slowly in it compared to soil.[87] Five samples were tested over 30 days: MCC (control), latex, HTW, and composite electrodes TWL0G and TWL20G, as shown in **Figure 3**. As expected, MCC showed significant biodegradability, starting to degrade from day 3 and reaching a final BOD of 33.6 mg O_2/100 mg material by day 30, consistent with its known high degradability.[88] Latex exhibited delayed and lower degradation, starting around day 8 and stabilizing at 4.7 mg O_2/100 mg by day 30. HTW began to degrade on day 1 and reached a plateau around 25 mg O_2/100 mg by day 20, showing very high biodegradability. The TWL0G electrode began to degrade on day 2 and reached 25.6 mg O_2/100 mg by day 30, closely matching the trend of HTW. The TWL20G sample followed a similar degradation pattern and reached a final BOD of 27.3 mg O_2/100 mg. The value of BOD obtained is higher or comparable with similar previous work involving biopolymer-based composites containing GnP.[2,6]

To assess how water absorption influences conduction mechanisms, the sheet resistance values of the various compositions were measured both in dried conditions, immediately after curing at 50 ° C for 24 h, and in standard ambient conditions (20 °C and 50% RH). The results are shown in **Table 2**.

The resistivity values were calculated considering the thicknesses of the film which was around 160 µm. Under standard conditions, it was observed that the sample with 0% GnPs displayed a resistivity of 3220.32 ± 115.27 Ωm, while samples with 5% and 10% GnPs exhibited resistivity values of 1084.16 ± 720.50 Ωm and 694.95 ± 45.74 Ωm, respectively. As the GnPs concentration increased to 20%, the resistivity significantly decreased, reaching 0.51 ± 0.16 Ωm.

The resistivity values for Latex, TWL0G, TWL5G, and TWL10G under dry conditions exceeded the upper measurement limit of the two-probe step (approximately 100 MΩ). This indicate that these samples did not reach the electronic percolation threshold, and their conductivity under ambient conditions is primarily governed by ionic transport through absorbed moisture. After the 24 h drying step at 50 °C, the removal of moisture eliminated these ionic pathways, and the films behaved as insulators, with resistivity values beyond the detection range of the instrument. In contrast, the TWL20G sample, which contained 20 wt% GnPs, remained conductive after drying. Notably, the sample TWL20G showed identical resistivity values within the error margins for both ambient and dry conditions, as confirmed by the ANOVA analysis (p-value at 95% confidence). This, together with the lack of conductivity in the dried samples at lower GnPs loadings, demostrated that electronic conduction is dominant at the highest GnPs concentration. Thus, at 20 wt. conductivity is primarily governed by electron transport through a percolated GnP network, with negligible contribution from moisture.

In particular, referring to latex-based matrix enriched with graphene-related materials like our system, it is possible to find examples with lower or higher resistivity values in the literature. For instance, Kitsawat et al.[89] reached a resistivity of 45 Ω m while Noël et al.[90] of 0.01 Ω m.

To evaluate the practical application of this composite material as a conductor, we used TWL20G as a bioimpedance electrode. TWL20G was selected as the sample with best compromise between conductivity, mechanical integrity, and processability for the intended application. Despite its resistivity of approx. 0.46 Ωm, higher than the typical range for commercial ECG electrodes (approx. 0.10 Ωm), which were used as a control, TWL20G was chosen for its biodegradability, flexibility, and potential for sustainable bioelectronics. Two dry TWL20G electrodes (without conductive gel) were applied directly to a biological specimen (a banana), as detailed in the methodology section. For comparison, two ECG electrodes were applied to a separate banana. Since dry TWL20G electrodes are less conductive than ECG electrodes, which also contain conductive gel for enhanced ion transfer, they initially registered a higher impedance magnitude. However, both electrode types exhibited a gradual decrease in impedance over time, likely due to improved electrode-skin contact **Figure 4a**. Measurements taken at t0 (initial), t1 (after

Table 2. Average resistivity of the films with varying GnPs % under ambient room conditions and dry conditions, including standard deviation and ANOVA test results for each group. Lowercase letters in the ANOVA column indicate significant differences between groups, with different letters denoting statistically different results at a 95% confidence level.

Condition	Sample	Resistivity [Ωm]	SD ±	ANOVA
Room conditions (20 °C, 50% RH)	Latex	above instrument limit	–	–
	TWL0G	3320.32	115.27	a
	TWL5G	1084.16	720.50	b
	TWL10G	694.95	45.74	bc
	TWL20G	**0.51**	**0.16**	c
Dry condition (50 °C for 24h)	Latex	above instrument limit	–	–
	TWL0G	above instrument limit	–	–
	TWL5G	above instrument limit	–	–
	TWL10G	above instrument limit	–	–
	TWL20G	**0.46**	**0.39**	c

5 min), and t4 (after 20 min) show a stabilization trend. This phenomenon, observed in both TWL20G and ECG electrodes, is common in bioimpedance measurements, where initial fluctuations occur due to electrode polarization and the settling of the electrode-tissue interface.[91] For ECG electrodes, impedance magnitude is initially higher at t0, decreases at t1, and stabilizes by t4, reflecting the natural equilibration process over time. A similar trend was observed for TWL20G, though the changes were less pronounced. As the electrodes establish a more consistent contact with the specimen, measurement reliability improves. The phase response of both electrodes was frequency-dependent. At lower frequencies, the ECG electrode's phase increased from t0 to t4 Figure 4b, while the TWL20G electrode's phase decreased Figure 4b, with these trends reversing at higher frequencies. These phase variations likely result from differences in capacitive and polarization behavior between gel-based and dry electrodes.[91]

In particular, TWL20G being a dry, composite electrode may have different interfacial capacitance and surface characteristics compared to pre-gelled ECG electrodes. These material-specific factors influence charge distribution and polarization, explaining the distinct phase response observed in Figure 4b.

Despite these differences, the overall trends in the Bode plots were similar for both electrode types. Both exhibited higher impedance magnitudes at lower frequencies, lower magnitudes at higher frequencies, and a characteristic capacitive peak in phase angle at medium frequencies. These trends, typical of biological tissues,[92] confirm the suitability of the proposed electrodes for bioimpedance measurements on fruits.

While ECG electrodes were used as a standard benchmark, it is important to note that, to the best of our knowledge, plant-based electrodes, particularly those made from unextracted agricultural waste, have not yet been applied to bioimpedance measurements. As such, direct comparisons with similar materials are currently limited.

Finally, the TWL20G films were employed as bioimpedance electrodes to track the electrical impedance of a banana over the course of a week, to evaluate the electrode potential for both a long term use and for a use-case application. The data, depicted in Figure 4c, were collected every 5 min at a fixed 1 kHz frequency following a few hours of stabilization time. Here, it is possible to highlight two different behaviors. First, a rise in the banana's bioimpedance over time, which potentially corresponds with its ripening process. This finding is consistent with a prior study,[93] which has shown that the impedance of bananas increases as they ripen due to changes in their internal structure and composition, such as starch conversion to sugar and cell membrane degradation. Additionally, it may also be influenced by the electrode-skin interface deteriorating over time, as banana skin tends to shrink due to water loss during aging. Moreover, a daily fluctuation in the fruit bioimpedance magnitude, likely influenced by temperature variations between day and night, is observed in Figure 4c. This behavior is potentially temperature-dependent and has been discussed in the review.[94]. While not the focus of this study, further investigations are needed to monitor and optimize fruit temperature for applications such as storage and transport.

These results highlight the potential effectiveness, as a proof of concept, of using TW, represented by TWL20G films, as promising bioimpedance electrodes.

3. Conclusion

This study successfully developed conductive composites for electronics, integrating the principles of the circular economy to minimize the environmental impact of electronic waste and agricultural residues. The composites, formed by incorporating graphene nanoplatelet fillers into a latex-hydrolyzed tomato waste biobased matrix, demonstrated notable improvements in moisture uptake and electrical performance. Specifically, moisture absorption was reduced to 40% of the initial dry weight after 7 days, compared to 70% in pure hydrolyzed tomato waste films. Electrical characterization under both dry and humid conditions revealed stable resistivity (0.46 Ωm) at 20% GnPs concentration, with conduction primarily governed by electrons. Their functionality was validated in a practical application, where the composites served as bioimpedance electrodes for fruit monitoring, maintaining effective performance for over 170 continuous hours with impedance values comparable to conventional ECG electrodes.

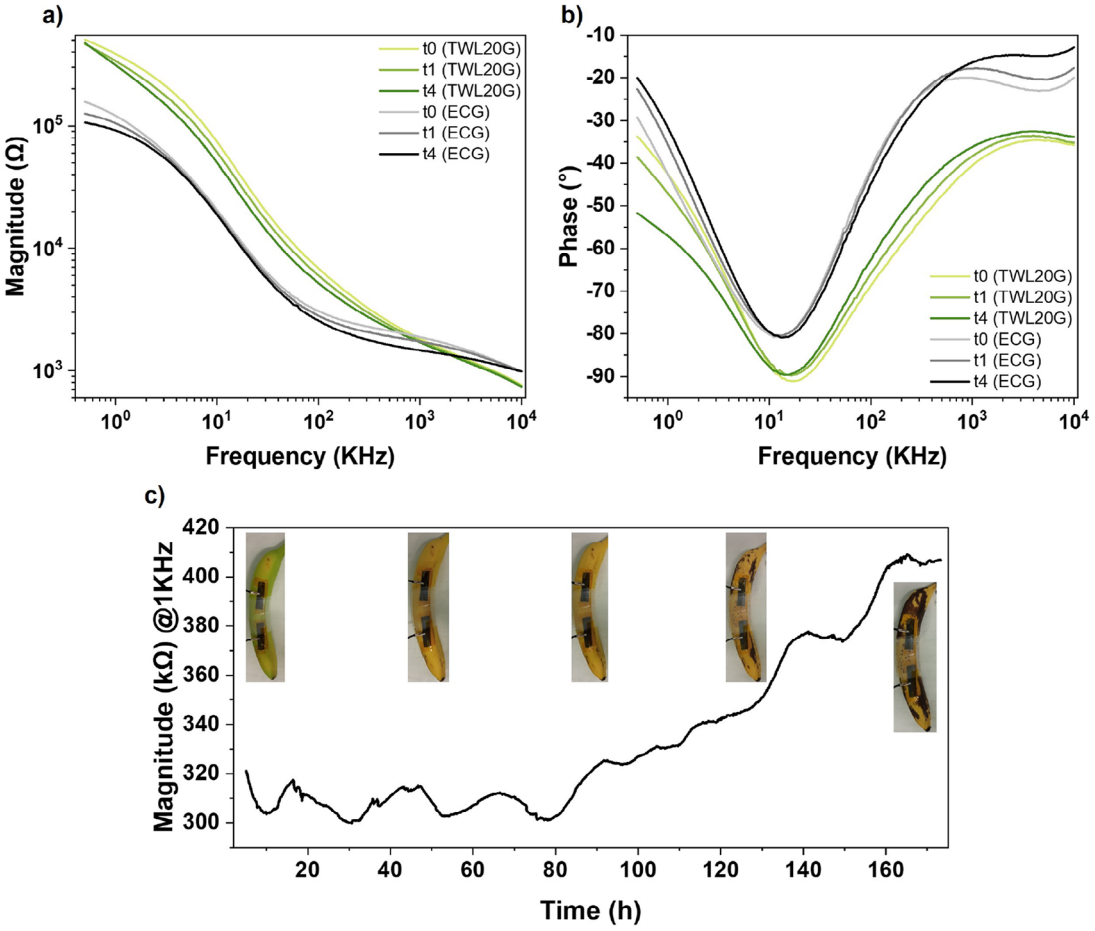

Figure 4. Proof-of-concept for using TWL20G as an electrode in bioimpedance measurements. a,b) Bode plots of banana bioimpedance using TWL20G and ECG electrodes, measured at three different time points: t0 (initial), t1 (5 min), and t4 (20 min). a) Impedance magnitude, b) Phase degree. c) Bioimpedance measurements taken every 5 minutes with TWL20G electrodes at 1 kHz over 1 week.

In addition to their functional properties, the composites exhibited biodegradability, reinforcing their potential as sustainable materials. The TWL20G sample began to degrade on day 1 and reached a final value of 27 (mgO_2/100 mgmaterial), highlighting their environmentally friendly nature. Although these results underscore the promise of waste-derived conductive materials, these composites have certain limitations. The materials demonstrate improved moisture resistance; nevertheless, they still absorb some water, which can affect their long-term stability (i.e., months) in humid environments. Another challenge is the variability of the composition of agricultural waste, which can introduce inconsistencies in the properties of the material between different batches. Further refinement of processing techniques and standardization of raw materials could mitigate these issues.

Future research should focus on optimizing the formulation and processing of the composites to enhance moisture resistance and standardization. One potential approach is surface treatments or coatings that could improve moisture resistance, extending the application range of these materials in various electronic and biomedical applications. Integrating these biocomposites into fully sustainable electronic devices, such as transient or biodegradable sensors, could pave the way for new eco-friendly technologies, reducing the environmental footprint of electronic components while promoting circular economy principles.

Overall, this study provides a proof-of-concept for utilizing agricultural waste in electronic applications, demonstrating a sustainable alternative to conventional conductive materials.

4. Experimental Section

Materials: TW postharvest stems were provided by Serenissima Ristorazione Spa (Liguria, Italy). 1 g of tomato waste powder was treated with 20 mL of 1 M ammonia solution (prepared from commercial ammonium hydroxide, 28–30% NH_3, Sigma-Aldrich, Cat. No. 221228) under continuous stirring at 40 °C for 24 h.

Natural rubber was sourced from Trustleaf (Cambridgeshire, United Kingdom), while GnPs (6–8 nm thick X 5 microns wide) were obtained from Strem Chemicals, Inc. (Massachusetts, United States).

Tomato Waste Pre-Treatment: The TW stems were dried in an oven at 40 °C for 24 h. Subsequently, the dried stems were mechanically ground using a Oster Versa 1400 blender (Georgia, United States), and the resulting material was pulverized and sieved with a Endecotts Minor 200 siever (Lombardy, Italy) to achieve a particle size below 50 µm. The obtained TW powder was subjected to hydrolysis with a 1M aqueous solution of ammonia (NH_3) stirring at 40 °C for 24 h, following procedures reported in previous studies.[13,64–66,95,96]

Bioplastics Preparation: Following hydrolysis, the HTW was mixed with latex in equal weight ratios. GnPs were incorporated into the mixtures at 0, 5, 10, and 20 wt.% concentrations to impart conductive properties. The mixtures were sonicated in a bath sonicator for 30 min at a frequency of 59 KHz, then allowed to rest briefly to eliminate air bubbles, which should be avoided to ensure a smooth film surface. Subsequently, the mixtures were cast into Teflon-coated Petri dishes and allowed to air-dry under ambient conditions until solvent evaporation was complete. A schematic representation of the bioplastic preparation process is presented in Figure 1a. And the component percentages in samples are shown in Table 1.

Methods: At least three different samples were tested for each measurement performed unless specified differently.

Attenuated Total Reflection-Fourier Transform Infrared (ATR-FTIR) Spectroscopy: ATR-FTIR spectroscopy was conducted using a Vertex 70v Bruker (Massachusetts, United States) spectrophotometer equipped with a diamond crystal ATR accessory. Spectra were recorded over the range of 4000–600 cm^{-1}, with a resolution of 2 cm^{-1}, using 32 scans per sample. Baseline correction of the spectra was performed using OPUS software to ensure the accuracy of the measurements.

Profilometer: The surface roughness of the films was evaluated using a Zeta-20 optical profilometer (California, United States). This non-contact method provided precise surface topography measurements, allowing for the quantification of surface roughness across the film specimens.

Scanning Electron Microscopy (SEM): The structural characteristics of the composite films were analyzed using a JEOL JSM-6490LA (Tokyo, Japan) scanning electron microscope, equipped with a tungsten thermionic electron source. The microscope was operated under high-vacuum conditions at an acceleration voltage of 10 kV and a beam current of 78–80 μA. To preserve the films' original morphology, specimens were cryogenically treated with liquid nitrogen prior to cross-sectional analysis. The samples were then mounted on aluminum stubs using carbon tape. For enhanced conductivity and improved imaging quality, a gold coating approximately 10 nm thick was deposited on the samples using a Cressington 208HR Sputter Coater (Hertfordshire, United Kingdom).

Mechanical Properties: Uniaxial tensile tests were performed using an Instron 3365 universal testing machine (Norwood, MA, USA). Prior to testing, samples were conditioned in a climatic chamber at 50% relative humidity and 25°C for 24 h. The specimens were shaped in a dog-bone geometry with a length of 25 mm and a width of 3.9 mm in the gauge section. The distance between grips was set at 3.5 mm, and tests were conducted at a constant crosshead speed of 3 mm/min. Key mechanical parameters, including elongation at break (%), Young's modulus (MPa), and tensile strength (MPa), were calculated from the resulting stress-strain curves. At least 10 replicates were evaluated and results are expressed as mean ± standard deviation.

Moisture Absorption: The conditioning procedure for the films entailed initial drying to remove moisture using a Memmert oven (Bavaria, Germany). Subsequently, the films were subjected to humidity absorption assessment by placement within a glass vial held at a constant relative humidity of 100% and the tare weight (W_{tare}) of each vial was recorded prior to sample placement. The initial weight of the samples (W_0) was calculated by subtracting W_{tare} from the total weight on day 0. Weight alterations (W_t) were monitored daily, and the percentage humidity uptake was calculated using:

$$\text{Humidity Uptake}(\%) = \left(\frac{W_t - W_0}{W_0}\right) \times 100 \quad (1)$$

These measurements quantified the progressive uptake of water over the experimental duration.

Water Contact Angle: The water contact angles of the bioplastics were measured using an OCA 20 contact angle goniometer from (DataPhysics Instruments GmbH, Filderstadt, Germany), at room temperature. A droplet of deionized water measuring 5 μL was carefully placed onto the surface of each film. The contact angles were determined by capturing side-view images of the droplets, with measurements analyzed using the accompanying software.

Biochemical Oxygen Demand: Biodegradation in water was assessed by measuring the BOD using the OxiTop-IDS system (Xylem Analytics, New York, USA). Experiments were conducted in hermetically sealed dark glass bottles containing 432 mL of seawater from the Port of Genoa along with defined quantities (in the order of 100 mg) of each sample. Sodium hydroxide was used to capture carbon dioxide generated during biodegradation. Oxygen consumption in the free volume of the bottles was recorded based on the pressure decrease. Raw oxygen consumption data (mg O_2/L) were corrected by subtracting the mean values of blanks, which were obtained from seawater without test samples. The corrected values were normalized to the sample mass and expressed as mg O_2/100 mg of the sample.

Electrical Properties: Sheet resistance measurements were conducted utilizing a two-probe resistance analyzer (Signatone 1160 probe station, Lucas Signatone Corporation, California, USA) in conjunction with a Keithley 2611A sourcemeter (Keithley Instruments, Ohio, USA). Two-probe measurements were utilized since the measured resistance was greater than kΩ, and thus the contact resistance was negligible, avoiding the need for a four-probe setup. A voltage range spanning from −1 to 1 volt was applied across samples containing varying proportions of GnPs. Electrodes composed of silver paste (RS Pro, Volume resistivity 0.001 (Ωm) cm) were applied onto the specimens surface, maintaining a separation distance of 5 mm. The sheet resistance of the films was measured under either ambient conditions or after drying the same samples in an oven by subjecting them to a temperature of 50 °C for a duration of 24 h. Then, considering the thickness of the materials, it was converted to resistivities.

Electrical Impedance Measurements: Electrical impedance was measured using a semi-portable impedance analyzer (Digilent Analog Discovery 2) (Digilent Inc., Washington, USA) across a frequency range from 100 Hz to 10 MHz. The measurement was conducted at 200 logarithmically spaced frequency points with a two-electrode setup. To compensate the electrode effect on the measurement, especially at high and low frequencies and considering the use of custom-made electrodes, the system was calibrated by means of a open/short calibration procedure. Continuous measurements were carried out for a period of 7 days with 5-min acquisition interval, through the WaveForms script editor of the instrument. Bioimpedance assessments were performed on a banana fruit utilizing the TWL20G samples as dry electrodes, devoid of gel or conductive paste. These electrodes adhered to specified dimensions (3.6 × 1.2 cm) with a 2 cm inter-electrode distance, and were secured in place using parafilm (measuring 10 × 5 cm) to allow for both a good electrical contact and insulation from the environment. To ensure consistency, the same individual applied the electrodes, thereby minimizing variations in pressure and bias. ECG electrodes served as a control in the experiment. Two pre-gelled ECG (Ag/AgCl) Arbo H124SG electrodes (Medtronic, Minnesota, USA), placed on the same fruit with equal spacing (i.e., 2 cm), were applied as a control, to validate the obtained impedance spectra.

Statistical Analysis: Descriptive statistics, including the mean and standard deviation, were calculated, followed by a one-way analysis of variance (ANOVA) to assess significant differences among treatment means at a significance level of $p < 0.05$. Tukey's post-hoc test was used for pairwise comparisons to identify specific differences between groups, using OriginPro (Version 2021. OriginLab Corporation, Massachusetts, USA). A grouping letter system was applied to categorize treatments based on statistical similarity. Treatments sharing the same letter are not significantly different, while different letters indicate significant differences in means. For Figure 4c, data were processed and visualized using *R* (4.4.0)[97] and the RStudio platform (2024.12.0).[98]

Supporting Information

Supporting Information is available from the Wiley Online Library or from the author.

Acknowledgements

D.M. and P.C. contributed equally to this work. The authors gratefully acknowledge the co-funding of this work by the Free University of Bozen-Bolzano and the Istituto Italiano di Tecnologia (IIT). The authors acknowledge the help of Dr. Gabriele Nanni from the Smart Materials laboratory for producing the BOD data presented in Figure 3. This work was supported by the Open Access Publishing Fund of the Free University of Bozen-Bolzano. P. C. acknowledges funding from the Marie Skłodowska-Curie actions (project name: BioConTact, Grant Agreement No. 101022279) under the European Union's Horizon 2020 research and innovation programme. D. M. gratefully acknowledges financial support from the European Union's Horizon Europe research and innovation program under the Marie Skłodowska-Curie grant agreement No. 101103474. Figure 1a was created with Biorender. This work was funded also by the European Union - NextGenerationEU and by the Ministry of University and Research (MUR), National Recovery and Resilience Plan (NRRP), Mission 4, Component 2, Investment 1.5, project "RAISE - Robotics and AI for Socio-economic Empowerment" (ECS00000035). [Correction added on August 12, 2025, after first online publication: the authors added a sentence in this version.]

Conflict of Interest

The authors declare no conflict of interest.

Data Availability Statement

The data that support the findings of this study are available from the corresponding author upon reasonable request.

Keywords

bioimpedence, circular economy, sustainable electronics, latex, tomato waste

Received: February 10, 2025
Revised: May 12, 2025
Published online: July 18, 2025

[1] M. Irimia-Vladu, *Chem. Soc. Rev.* **2014**, *43*, 588.
[2] R. Arbaud, M. Najafi, J. M. Gandarias, M. Lorenzini, U. C. Paul, A. Zych, A. Athanassiou, P. Cataldi, A. Ajoudani, *Adv. Mater. Technol.* **2024**, *9*, 2301265.
[3] A. Honarbari, P. Cataldi, A. Zych, D. Merino, N. Paknezhad, L. Ceseracciu, G. Perotto, M. Crepaldi, A. Athanassiou, *ACS Appl. Electron. Mater.* **2023**, *5*, 5050.
[4] C. P. Baldé, R. Kuehr, T. Yamamoto, R. McDonald, E. D'Angelo, S. Althaf, G. Bel, O. Deubzer, E. Fernandez-Cubillo, V. Forti, V. Gray, S. Herat, S. Honda, G. Iattoni, D. S. Khetriwal, V. L. di Cortemiglia, Y. Lobuntsova, I. Nnorom, N. Pralat, M. Wagner, *Global E-waste Monitor 2024*, Geneva/Bonn, **2024**.
[5] G. Cantarella, M. Madagalam, I. Merino, C. Ebner, M. Ciocca, A. Polo, P. Ibba, P. Bettotti, A. Mukhtar, B. Shkodra, A. K. M. S. Inam, A. J. Johnson, A. Pouryazdan, M. Paganini, R. Tiziani, T. Mimmo, S. Cesco, N. Münzenrieder, L. Petti, N. Cohen, P. Lugli, *Adv. Funct. Mater.* **2023**, *33*, 2210422.
[6] G. Spallanzani, M. Najafi, M. Zahid, E. L. Papadopoulou, L. Ceseracciu, M. Catalano, A. Athanassiou, P. Cataldi, A. Zych, *Adv. Sustainable Syst.* **2023**, *7*, 2300220.
[7] X. Wu, P. Steiner, T. Raine, G. Pinter, A. Kretinin, C. Kocabas, M. Bissett, P. Cataldi, *Adv. Electron. Mater.* **2020**, *6*, 2000232.
[8] N. Karić, A. S. Maia, A. Teodorović, N. Atanasova, G. Langergraber, G. Crini, A. R. Ribeiro, M. olić, *Chemical Engineering Journal Advances* **2022**, *9*, 100239.
[9] B. Wu, J. Li, Z. Yao, X. Li, W. Wang, Z. Wu, Q. Zhou, *Sci. Total Environ.* **2023**, *905*, 167235.
[10] R. Lan, S. D. Eastham, T. Liu, L. K. Norford, S. R. Barrett, *Nat. Commun.* **2022**, *13*, 6537.
[11] Q. Jin, L. Yang, N. Poe, H. Huang, *Trends Food Sci. Technol.* **2018**, *74*, 119.
[12] P. K. Sarangi, M. M. Nayak, *Liquid biofuels: Fundamentals, characterization, and applications* **2021**, 697.
[13] D. Merino, A. I. Quilez-Molina, G. Perotto, A. Bassani, G. Spigno, A. Athanassiou, *Green Chem.* **2022**, *24*, 4703.
[14] Z. Mengqi, A. Shi, M. Ajmal, L. Ye, M. Awais, *Biomass Convers. Biorefin.* **2021**, 1.
[15] E. Aprianti, P. Shafigh, S. Bahri, J. N. Farahani, *Constr. Build. Mater.* **2015**, *74*, 176.
[16] X. Sun, Z. Dou, G. C. Shurson, B. Hu, *Resour., Conserv. Recycl.* **2024**, *201*, 107325.
[17] R. Kamel, N. A. El-Wakil, A. Dufresne, N. A. Elkasabgy, *Int. J. Biol. Macromol.* **2020**, *163*, 1579.
[18] P. Rao, V. Rathod, *Chem. Rec.* **2019**, *19*, 1858.
[19] P. Cataldi, O. Condurache, D. Spirito, R. Krahne, I. S. Bayer, A. Athanassiou, G. Perotto, *ACS Sustainable Chem. Eng.* **2019**, *7*, 12544.
[20] Z. Su, Y. Yang, Q. Huang, R. Chen, W. Ge, Z. Fang, F. Huang, X. Wang, *Prog. Mater. Sci.* **2022**, *125*, 100917.
[21] T. Li, C. Chen, A. H. Brozena, J. Zhu, L. Xu, C. Driemeier, J. Dai, O. J. Rojas, A. Isogai, L. Wågberg, L. Hu, *Nature* **2021**, *590*, 47.
[22] B. Thomas, M. C. Raj, J. Joy, A. Moores, G. L. Drisko, C. Sanchez, *Chem. Rev.* **2018**, *118*, 11575.
[23] F. Hoeng, A. Denneulin, J. Bras, *Nanoscale* **2016**, *8*, 13131.
[24] J. Tao, Z. Fang, Q. Zhang, W. Bao, M. Zhu, Y. Yao, Y. Wang, J. Dai, A. Zhang, C. Leng, D. Henderson, Z. Wang, L. Hu, *Adv. Electron. Mater.* **2017**, *3*, 1600539.
[25] J. Huang, H. Zhu, Y. Chen, C. Preston, K. Rohrbach, J. Cumings, L. Hu, *ACS nano* **2013**, *7*, 2106.
[26] S. Moreno, M. Baniasadi, S. Mohammed, I. Mejia, Y. Chen, M. A. Quevedo-Lopez, N. Kumar, S. Dimitrijevich, M. Minary-Jolandan, *Adv. Electron. Mater.* **2015**, *1*, 1500154.
[27] J. Jin, D. Lee, H.-G. Im, Y. C. Han, E. G. Jeong, M. Rolandi, K. C. Choi, B.-S. Bae, *Adv. Mater.* **2016**, *28*, 5169.
[28] Z. Wang, H. Wei, Y. Huang, Y. Wei, J. Chen, *Chem. Soc. Rev.* **2023**, *52*, 2992.
[29] Y. Zhu, R. Haghniaz, M. C. Hartel, L. Mou, X. Tian, P. R. Garrido, Z. Wu, T. Hao, S. Guan, S. Ahadian, H.-J. Kim, V. Jucaud, M. R. Dokmeci, A. Khademhosseini, *ACS Biomater. Sci. Eng.* **2021**, *9*, 2048.
[30] C. Cui, Q. Fu, L. Meng, S. Hao, R. Dai, J. Yang, *ACS Appl. Bio Mater.* **2020**, *4*, 85.
[31] Y. Zhang, Q. Tang, J. Zhou, C. Zhao, J. Li, H. Wang, *ACS Biomater. Sci. Eng.* **2023**, *10*, 191.
[32] P. Cataldi, J. A. Heredia-Guerrero, S. Guzman-Puyol, L. Ceseracciu, L. La Notte, A. Reale, J. Ren, Y. Zhang, L. Liu, M. Miscuglio, P. Savi, S. Piazza, M. Duocastella, G. Perotto, A. Athanassiou, I. S. Bayer, *Adv. Sustainable Syst.* **2018**, *2*, 1800069.
[33] X. Wang, Z. Bai, M. Zheng, O. Yue, M. Hou, B. Cui, R. Su, C. Wei, X. Liu, *J. Sci.: Adv. Mater. Devices* **2022**, *7*, 100451.
[34] R. Yin, C. Zhang, J. Shao, Y. Chen, A. Yin, Q. Feng, S. Chen, F. Peng, X. Ma, C.-Y. Xu, F. Liu, W. Zhao, *J. Mater. Sci. Technol.* **2023**, *145*, 83.
[35] D. Ji, J. M. Park, M. S. Oh, T. L. Nguyen, H. Shin, J. S. Kim, D. Kim, H. S. Park, J. Kim, *Nat. Commun.* **2022**, *13*, 3019.
[36] J. Hu, Z. Wang, Y. Si, C. Hong, C. Zhao, Y. Xing, W. Ling, Y. Wang, L. Feng, W. Feng, *J. Mater. Chem. A* **2023**, *11*, 878.
[37] X. Li, L. Jiang, M. Yan, H. Bi, Q. Wang, *Int. J. Biol. Macromol.* **2023**, *242*, 124780.

[38] M. Baumgartner, F. Hartmann, M. Drack, D. Preninger, D. Wirthl, R. Gerstmayr, L. Lehner, G. Mao, R. Pruckner, S. Demchyshyn, L. Reiter, M. Strobel, T. Stockinger, D. Schiller, S. Kimeswenger, F. Greibich, G. Buchberger, E. Bradt, S. Hild, S. Bauer, M. Kaltenbrunner, *Nat. Mater.* **2020**, *19*, 1102.
[39] A. Heiden, D. Preninger, L. Lehner, M. Baumgartner, M. Drack, E. Woritzka, D. Schiller, R. Gerstmayr, F. Hartmann, M. Kaltenbrunner, *Sci. Rob.* **2022**, *7*, eabk2119.
[40] P. Cataldi, L. Lamanna, C. Bertei, F. Arena, P. Rossi, M. Liu, F. Di Fonzo, D. G. Papageorgiou, A. Luzio, M. Caironi, *Adv. Funct. Mater.* **2022**, *32*, 2113417.
[41] L. You, X. Shi, J. Cheng, J. Yang, C. Xiong, Z. Ding, Z. Zheng, S. Wang, J. Wang, *J. Colloid Interface Sci.* **2022**, *625*, 197.
[42] S. Ding, Z. Jiang, F. Chen, L. Fu, Y. Lv, Y. Qian, S. Zhao, *ACS Appl. Mater. Interfaces* **2020**, *12*, 27572.
[43] K. Liang, Y. Chen, S. Wang, D. Wang, W. Wang, S. Jia, N. Mitsuzakic, Z. Chen, *J. Energy Storage* **2023**, *70*, 107947.
[44] N. Ahmad, A. Rinaldi, M. Sidoli, G. Magnani, V. Vezzoni, S. Scaravonati, L. Pasetti, L. Fornasini, H. Gupta, M. Tamagnone, F. Ridi, C. Milanese, M. Riccò, D. Pontiroli, *J. Power Sources* **2024**, *624*, 235511.
[45] N. Ahmad, A. Rinaldi, M. Sidoli, G. Magnani, A. Morenghi, S. Scaravonati, V. Vezzoni, L. Pasetti, L. Fornasini, F. Ridi, C. Milanese, M. Riccò, D. Pontiroli, *J. Energy Storage* **2024**, *99*, 113267.
[46] C. Zhan, X. Yu, Q. Liang, W. Liu, Y. Wang, R. Lv, Z.-H. Huang, F. Kang, *RSC advances* **2016**, *6*, 89391.
[47] N. Aprianti, A. Kismanto, N. K. Supriatna, S. Yarsono, L. M. T. Nainggolan, R. I. Purawiardi, O. Fariza, F. J. Ermada, P. Zuldian, A. A. Raksodewanto, R. Alamsyah, *Bioresour. Technol. Rep.* **2023**, 101587.
[48] L. Jiang, S. O. Han, M. Pirie, H. H. Kim, Y.-H. Seong, H. Kim, J. S. Foord, *Energy & Environment* **2021**, *32*, 1117.
[49] Z. Zou, C. Jiang, *J. Alloys Compd.* **2020**, *815*, 152280.
[50] L. Peng, Y. Liang, J. Huang, L. Xing, H. Hu, Y. Xiao, H. Dong, Y. Liu, M. Zheng, *ACS Sustainable Chem. Eng.* **2019**, *7*, 10393.
[51] W. Shi, B. Chang, H. Yin, S. Zhang, B. Yang, X. Dong, *Sustainable Energy Fuels* **2019**, *3*, 1201.
[52] X. Wei, B. Qiu, L. Xu, Q. Qin, W. Zhang, Z. Liu, F. Wei, Y. Lv, *J. Energy Storage* **2023**, *62*, 106900.
[53] Q. Chen, X. Tan, Y. Liu, S. Liu, M. Li, Y. Gu, P. Zhang, S. Ye, Z. Yang, Y. Yang, *J. Mater. Chem. A* **2020**, *8*, 5773.
[54] S. S. Shams, L. S. Zhang, R. Hu, R. Zhang, J. Zhu, *Mater. Lett.* **2015**, *161*, 476.
[55] E. Azwar, W. A. W. Mahari, J. H. Chuah, D.-V. N. Vo, N. L. Ma, W. H. Lam, S. S. Lam, *Int. J. Hydrogen Energy* **2018**, *43*, 20811.
[56] P. Chaudhary, S. Bansal, B. B. Sharma, S. Saini, A. Joshi, *J. Energy Storage* **2024**, *78*, 109996.
[57] Y.-L. Bai, C.-C. Zhang, F. Rong, Z.-X. Guo, K.-X. Wang, *Chem. - Eur. J.* **2024**, *30*, e202304157.
[58] V. Molahalli, A. Sharma, K. Bijapur, G. Soman, N. Chattham, G. Hegde, *Mater. Today Commun.* **2024**, 108034.
[59] Y. Chen, X. Wang, X. Wang, *Energy Technol.* **2024**, 2301436.
[60] H. Ling, R. Chen, Q. Huang, F. Shen, Y. Wang, X. Wang, *Green Chem.* **2020**, *22*, 3208.
[61] J. Lv, Y. Dai, H. Xu, Y. Zhong, L. Zhang, Z. Chen, X. Sui, X. Feng, B. Wang, Z. Mao, *J. Mater. Chem. C* **2020**, *8*, 1309.
[62] J. M. Chang, I. J. Joye, *Waste Manage.* **2024**, *190*, 88.
[63] C. Pane, G. Celano, A. Piccolo, D. Villecco, R. Spaccini, A. M. Palese, M. Zaccardelli, *Chemical and Biological Technologies in Agriculture* **2015**, *2*, 1.
[64] D. Merino, A. Athanassiou, *Chem. Eng. J.* **2023**, *454*, 140171.
[65] D. Merino, R. Simonutti, G. Perotto, A. Athanassiou, *Green Chem.* **2021**, *23*, 5956.
[66] J. D. Estrada-Sotomayor, Ł. Łopusiewicz, E. Lizundia, S. Guenther, D. Merino, *Green Chem.* **2025**.
[67] P. Cataldi, A. Athanassiou, I. S. Bayer, *Appl. Sci.* **2018**, *8*, 1438.
[68] P. Cataldi, P. Steiner, M. Liu, G. Pinter, A. Athanassiou, C. Kocabas, I. A. Kinloch, M. A. Bissett, *Adv. Funct. Mater.* **2023**, *33*, 2301542.
[69] G. Fuertes, I. Soto, R. Carrasco, M. Vargas, J. Sabattin, C. Lagos, *J. Sens.* **2016**, *2016*, 4046061.
[70] M. E. Genovese, S. Abraham, G. Caputo, G. Nanni, S. K. Kumaran, C. D. Montemagno, A. Athanassiou, D. Fragouli, *ACS omega* **2018**, *3*, 13484.
[71] P. Ibba, M. Crepaldi, G. Cantarella, G. Zini, A. Barcellona, M. Petrelli, B. D. Abera, B. Shkodra, L. Petti, P. Lugli, in *2020 IEEE International Symposium on Circuits and Systems (ISCAS)*, IEEE, **2020**, pp. 1–5.
[72] P. Ibba, G. Cantarella, B. D. Abera, L. Petti, A. Falco, P. Lugli, in *International Conference on Electrical Bioimpedance*, Springer Singapore Singapore, **2019**, pp. 25–32.
[73] S. Hamed, P. Ibba, A. Altana, P. Lugli, L. Petti, in *2023 IEEE Conference on AgriFood Electronics (CAFE)*, IEEE, **2023**, pp. 20–24.
[74] S. Hamed, A. Altana, P. Lugli, L. Petti, P. Ibba, *Comput. Electron. Agric.* **2024**, *226*, 109347.
[75] A. Altana, S. Hamed, P. Lugli, L. Petti, P. Ibba, *IEEE Trans. AgriFood Electronics* **2024**.
[76] P. Ibba, A. Falco, A. Rivadeneyra, P. Lugli, in *2018 IEEE sensors*. IEEE, **2018**, pp. 1–4.
[77] A. Gent, S. Kawahara, J. Zhao, *Rubber Chem. Technol.* **1998**, *71*, 668.
[78] S. Rolere, S. Liengprayoon, L. Vaysse, J. Sainte-Beuve, F. Bonfils, *Polym. Test.* **2015**, *43*, 83.
[79] D. Merino, A. Athanassiou, *Adv. Sustainable Syst.* **2023**, *7*, 2300179.
[80] P. Sayfo, D. Pirityi, K. Pölöskei, *Mater. Today Chem.* **2023**, *29*, 101397.
[81] S. S. A. Kumar, M. N. Badawi, K. K. Kandiah, K. Ramesh, S. Ramesh, S. Tiong, *FlatChem* **2024**, 100758.
[82] C. Zhuang, R. Tao, X. Liu, L. Zhang, Y. Cui, Y. Liu, Z. Zhang, *Diamond Relat. Mater.* **2021**, *116*, 108438.
[83] H. Zhang, W. Xing, H. Li, Z. Xie, G. Huang, J. Wu, *Adv. Ind. Eng. Polym. Res.* **2019**, *2*, 32.
[84] S. Bao, X. Yang, Z. Yu, Y. Shi, Y. Lu, *Green Energy Environ.* **2024**.
[85] M. Liu, P. Cataldi, R. J. Young, D. G. Papageorgiou, I. A. Kinloch, *Compos. Sci. Technol.* **2021**, *202*, 108592.
[86] M. Ahmad, M. Ridzuan, M. Abdul Majid, S. Sapuan, A. Shahriman, F. Mat, *J. Inorg. Organomet. Polym. Mater.* **2023**, *33*, 1802.
[87] A. Chamas, H. Moon, J. Zheng, Y. Qiu, T. Tabassum, J. H. Jang, M. Abu-Omar, S. L. Scott, S. Suh, *ACS Sustainable Chem. Eng.* **2020**, *8*, 3494.
[88] V. Galli, V. F. Annese, G. Coco, P. Cataldi, V. Scribano, I. K. Ilic, A. Athanassiou, M. Caironi, *Adv. Mater. Technol.* **2024**, 2400715.
[89] V. Kitsawat, S. Siri, M. Phisalaphong, *Polymers* **2024**, *16*, 288.
[90] A. Noël, J. Faucheu, J.-M. Chenal, J.-P. Viricelle, E. Bourgeat-Lami, *Polymer* **2014**, *55*, 5140.
[91] O. G. Martinsen, A. Heiskanen, *Bioimpedance and bioelectricity basics*, Elsevier, **2023**.
[92] P. Ibba, Ph.D. thesis, Free University of Bozen-Bolzano, **2021**.
[93] A. Chowdhury, T. Bera, D. Ghoshal, B. Chakraborty, in *Proceedings of the 2015 Third International Conference on Computer, Communication, Control and Information Technology (C3IT)*. IEEE, **2015**, pp. 1–4.
[94] U. Pliquett, *Food Eng. Rev.* **2010**, *2*, 74.
[95] D. Merino, L. Bertolacci, U. C. Paul, R. Simonutti, A. Athanassiou, *ACS Appl. Mater. Interfaces* **2021**, *13*, 38688.
[96] D. Merino, A. Athanassiou, *ACS Sustainable Chem. Eng.* **2022**, *10*, 10789.
[97] R. C. Team, et al., R: A language and environment for statistical computing, *Foundation for Statistical Computing, Vienna, Austria* **2013**, https://citeseerx.ist.psu.edu/document?repid=rep1&type=pdf&doi=bc748aec2bcc46eb319d5446da614b37729e9dbe.
[98] R. S. Team, RStudio: integrated development environment for R, *(No Title)* **2021**.